Selective pumping and spatial hole burning for generation of photon wave packets with ray-wave duality in solid-state lasers

J C Tung[1], **H C Liang**[2], **P H Tuan**[1], **F L Chang**[1], **K F Huang**[1], **T H Lu**[3] and **Y F Chen**[1]

[1] Department of Electrophysics, National Chiao Tung University, 1001 Ta-Hsueh Rd., Hsinchu 30010, Taiwan
[2] Institute of Optoelectronic Science, National Taiwan Ocean University, 2 Pei-Ning Rd., Keelung 20224, Taiwan
[3] Department of Physics, National Taiwan Normal University, 88 Ting-Chou Rd., Sec. 4, Taipei 11677, Taiwan

E-mail: yfchen@cc.nctu.edu.tw

Abstract

The selective pumping and the spatial hole burning are thoroughly considered to determine the excited transverse and longitudinal eigenmodes. By using the mode locking of the excited eigenmodes, an analytical wave representation is derived to manifest the ray-wave duality of the optical wave packet dynamics in the laser resonator. The derived wave function is employed to extract the parametric formula for the periodic ray orbits that reveal the subtle origin between the hyperbolic caustics and linear trajectories. Moreover, the temporal dynamics of the output beam for the total mode-locked state is theoretically demonstrated by combining with the parametric formula and the derived wave function. More importantly, an experiment based on the self-mode-locked laser is performed to make a comparison with theoretical analysis.

Keywords: selective pumping, spatial hole burning, mode locking

(Some figures may appear in colour only in the online journal)

I. Introduction

Spatial structures of laser modes in broad-area resonators have received much interest for a long time because they give a deep insight into pattern formation of natural waves [1–8]. Since the Schrödinger equation has the same mathematical form as the wave equation [9], many quantum signatures have been realized in optical context, such as quantum chaos phenomena [10, 11], disorder induced wave localization [12], geometric phases [13] and the issue of quantum tunneling [14]. Analogous to the particle-wave duality, a fundamental duality exists between ray and wave optics. Stationary lasing modes with spatial distributions localized on geometric rays have been experimentally observed in degenerate spherical cavities [15–18]. Furthermore, the representation of quantum

coherent states has been employed to elucidate the relationship between the geometric modes and Hermite-Gaussian (HG) eigenmodes [19].

From the ray-wave duality, it is expected that there are time-dependent wave packets with dynamical behaviors corresponding to the ray traces in geometric optics. The dynamics of photon wave packets inside optical resonators is intimately similar to that of quantum wave packets inside mesoscopic structures [9]. Time-dependent quantum wave packets localized on classical orbits play an indispensable role in the classical-quantum connection. It has been verified [20, 21] that quantum wave-packet coherent states are not only the most representative states related to the classical dynamics but also the most persistent states in the system interacting with the environment [22]. Furthermore, quantum wave packets associated with

classical orbits are widely used to explore diverse phenomena in solid-state physics, nuclear and atom physics [23–26]. Therefore, exploring the time-dependent photon wave packets in optical resonators can be an important platform in the light of mesoscopic phenomena and pattern formation in laser physics [9, 27]. In the experimental aspect, the generation of photon wave-packet states is associated with the total mode-locked operation that is the simultaneously longitudinal and transverse mode locking in laser resonators [28–30].

The Kerr-lens mode locking has been identified to be an extremely simple means of achieving the self-mode-locked operation [31]. The fundamental mechanism is to exploit the Kerr nonlinearity of the gain medium itself and the soft aperture formed by the pumped volume in the gain medium. Krausz *et al* [31] derived a simple criterion to analyze the self-starting threshold of the passive mode locking from mode beating fluctuations in a free-running solid-state laser. This criterion indicates that a decrease in the cavity round-trip time can significantly reduce the intensity needed for self-starting at a fixed nonlinearity. Recently, the self-mode-locked operations in short linear cavities have been extensively confirmed in the diode-end-pumping approach with Yb-doped [32–35] and Nd-doped [36–39] crystal lasers. In addition, the total mode locking has been experimentally observed in solid-state lasers with the selective pumping to generate the wave packet states that mimic the dynamics of optical rays in both space and time [40]. Even so, the relationship between the selective pumping in a linear cavity and the formation of time-dependent wave packets with ray-wave duality has not been theoretically explored as yet. This understanding of this relationship can provide a deep insight into the manipulation of the generalized wave-packet states in wave systems.

In this work, we theoretically show that the selective pumping can be linked to the generation of the Schrödinger coherent state for the transverse dimensions. On the other hand, the effect of spatial hole burning (SHB) is considered to develop a theoretical formula for analyzing the maximum number of longitudinal lasing modes in end-pumped lasers. We further combine the generation of the multi-transverse and multi-longitudinal modes to derive an analytical wave representation for expressing the time-dependent wave-packet state. The derived wave function can be exploited to obtain the parametric formula for the periodic trajectories in spherical cavities to reveal the subtle relationship between the hyperbolic caustics and linear rays. Moreover, the emission of the time-dependent wave-packet state from the output coupler can be shown to exhibit the characteristics of multiple Gaussian beams. By using the parametric formula and the developed wave function, the temporal dynamics of the multiple Gaussian beams can be numerically manifested. Finally, an experiment based on the diode-pumped solid-state laser is performed to obtain the total mode-locked operation for making a comparison with theoretical analysis.

II. Selective pumping and spatial hole burning

Without loss of generality, we consider the spherical cavity formed by a concave mirror with radius of curvature R at

$z = -L$ and a flat mirror at $z = 0$. The wave function of eigenmodes in a concave-flat cavity is given by [41]

$$\Phi_{n,m,\ell}(x, y, z, t) = \sqrt{2} \ \psi_{n,m}(x, y, z)$$
$$\times \ \sin\left[k_{n,m,\ell} \ \tilde{z} - (m + n + 1) \theta_G(z) \right] e^{-i\omega_{n,m,\ell} t} \quad (1)$$

where the transverse distribution $\psi_{n,m}(x, y, z)$ is the Hermite-Gaussian mode:

$$\psi_{n,m}(x, y, z) = \frac{\sqrt{2}}{w(z)} (2^{n+m} n! \ m! \ \pi)^{-1/2} \ e^{-(\tilde{x}^2 + \tilde{y}^2)/2} H_n(\tilde{x}) H_m(\tilde{y}) \quad (2)$$

$H_n(\cdot)$ is the Hermite polynomials, $\tilde{x} = \sqrt{2} \, x/w(z)$, $\tilde{y} = \sqrt{2} \, y/w(z)$, $\tilde{z} = z \ [1 + (x^2 + y^2)/2(z^2 + z_R^2)]$, $w(z) = w_0 \sqrt{1 + (z/z_R)^2}$, w_0 is the beam radius at the waist, $z_R = \pi \, w_0^2/\lambda$ is the Rayleigh range, $k_{n,m,\ell}$ is the eigenvalue of the wave number, $\omega_{n,m,\ell} = ck_{n,m,\ell}$ is the eigen-frequency, ℓ is the longitudinal mode index, n and m are the transverse mode indices, and $\theta_G(z) = \tan^{-1}(z/z_R)$ is the Gouy phase. For a concave-flat solid-state laser, the longitudinal and transverse mode separations are respectively given by $\Omega_L = c/2L$ and $\Omega_T = (\Omega_L/\pi)\cos^{-1}[1 - (L^*/R)]^{1/2}$, where $L = L_c + (n_r - 1)L_g$, $L^* = L_c + [(1/n_r) - 1]L_g$, L_c is the geometrical length of the cavity, L_g is the length of the gain material, and n_r is the refractive index of the gain medium. In terms of Ω_L and Ω_T, the eigenvalue $k_{n,m,\ell}$ is given by $k_{n,m,\ell} = (\pi/L) \ [\ell + (n + m + 1) (\Omega_T/\Omega_L)]$. The eigenmode in equation (1) can be divided into two waves traveling in opposite directions: $\Phi_{n,m,\ell} = [\Phi_{n,m,\ell}^{(+)} + \Phi_{n,m,\ell}^{(-)}]/\sqrt{2}$, where

$$\Phi_{n,m,\ell}^{(\pm)}(x, y, z, t) = \psi_{n,m}(x, y, z) e^{-i(m+n+1)[\theta_T^{(\pm)}(\tilde{z},t) \mp \theta_G(z)]}$$
$$\times e^{-i \ell \theta_L^{(\pm)}(\tilde{z},t)} e^{\pm i\pi/2} \quad (3)$$

$$\theta_L^{(\pm)}(\tilde{z}, t) = 2\pi\left(\frac{t}{t_r} \pm \frac{\tilde{z}}{2L}\right) \quad (4)$$

and

$$\theta_T^{(\pm)}(\tilde{z}, t) = (\Omega_T/\Omega_L) \ \theta_L^{(\pm)}(\tilde{z}, t). \quad (5)$$

Here $t_r = 2L/c$ is the round trip time of light within the cavity. The components of $\Phi_{n,m,\ell}^{(+)}$ and $\Phi_{n,m,\ell}^{(-)}$ denote the waves traveling backward and forward in the cavity, respectively.

The criterion for the self-starting derived by Krausz *et al* [31] is given by $(\kappa P_i)_{th} > t_r/[t_c \ln(N)]$, where κ is a characteristic of the Kerr nonlinearity used for passive mode locking, P_i is the circulating average intracavity power in the free running laser, N is the number of longitudinal lasing modes, t_r is the cavity round-trip time, and t_c is effective correlation time between the longitudinal modes in the free-running laser. It has been experimentally confirmed [32–39] that combining the Kerr nonlinearity of the laser crystal with the high-Q short cavity can directly lead to the phase locking between the excited modes. As a result, the general representation for the phase-locked states in a standing-wave cavity can be expressed as a sum of two traveling waves: $\Psi = [\Psi^{(+)} + \Psi^{(-)}]/\sqrt{2}$, where

$$\Psi^{(\pm)}(x, y, z, t) = \sum_{\ell=\ell_o}^{\ell_o+N-1} \sum_{n=0}^{\infty} \sum_{m=0}^{\infty} c_\ell \, a_{n,m} \, \Phi_{n,m,\ell}^{(\pm)}(x, y, z, t) \quad (6)$$
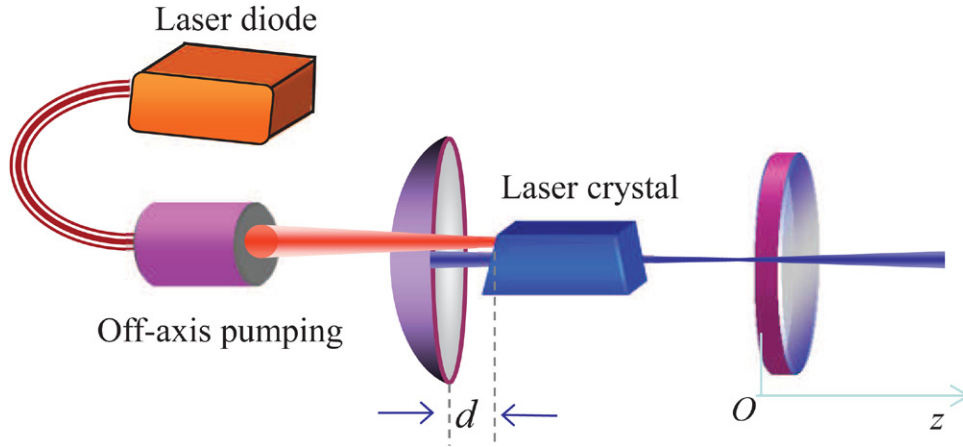
Figure 1. Experimental setup for the total mode-locked operation in a concave-flat cavity with the off-axis pumping scheme.

$a_{n,m}$ is the amplitude coefficient for the transverse order n and m, c_ℓ is the amplitude coefficient for the longitudinal order ℓ, the index ℓ_o indicates the minimum longitudinal order, and the integer N represents the total number of longitudinal eigenmodes in the lasing mode. It has been shown [42] that the coefficient $a_{n,m}$ is mainly controlled by the transverse overlap between the cavity mode $\psi_{n,m}(x, y, z)$ and the transverse distribution of the pump source $F(x, y)$, i.e.

$$a_{n,m} = \iint \psi_{n,m}(x, y, z_c) F(x, y) \mathrm{d}x \mathrm{d}y \tag{7}$$

where z_c is the location of the gain medium. For the end-pumping scheme, as shown in figure 1, the pump source $F(x, y)$ is assumed to a Gaussian distribution to derive a closed form for manifestation. Considering a selective pumping with the transverse displacements Δx and Δy in the x- and y-directions, the pump distribution $F(x, y)$ can be modeled as [42]

$$F(x, y) = \sqrt{\frac{2}{\pi w^2(z_c)}} \exp\left[-\frac{(x - \Delta x)^2 + (y - \Delta y)^2}{w^2(z_c)} \right] \tag{8}$$

Substituting equations (2) and (8) into equation (7) and using the generating function of the Hermite polynomials, the coefficient $a_{n,m}$ can be derived as [43]

$$a_{n,m} = \left[\frac{(n_o)^{n/2}}{\sqrt{n!}} \mathrm{e}^{-n_o/2} \right] \left[\frac{(m_o)^{m/2}}{\sqrt{m!}} \mathrm{e}^{-m_o/2} \right] \tag{9}$$

where $n_o = [\Delta x/w(z_c)]^2$ and $m_o = [\Delta y/w(z_c)]^2$. Note that the values of the parameters n_o and m_o signify the magnitudes of the off-axis displacements in the x- and y- directions, respectively. Equation (9) also indicates that the maximum contribution in the lasing mode comes from the eigenmode with the transverse indices n and m to be closest to the values n_o and m_o, respectively. For convenience, we take the parameters n_o and m_o to be the integers closest to the values of $[\Delta x/w(z_c)]^2$ and $[\Delta y/w(z_c)]^2$, respectively. Moreover, the expression in the square bracket of the equation (9) is just the form of the square root of the Poisson distribution.

With respect to the propagation along Oz axis of the resonator, we consider the SHB effect to explore the operation of the multiple longitudinal modes in a standing-wave cavity [44–49]. It is essentially confirmed that the stronger the SHB effect, the more the longitudinal lasing modes. In the end-pumping scheme, the strength of the SHB effect is primarily related to the separation d between the gain medium and the input mirror. Although the SHB effect has been widely discussed, here we originally derive an analytical formula to manifest the maximum number of longitudinal lasing modes as a function of the pump level and the crystal/mirror separation d. To derive the analytical formula, the variable z is changed into a new variable $z' = z + L$ to consider the round-trip gain of the Nth longitudinal lasing mode. For a gain medium located between $z' = d$ and $z' = d + L_g$, the round-trip gain of the Nth longitudinal mode can be expressed as [50]

$$g(N, d, P_{\mathrm{abs}}) = \left(\frac{P_{\mathrm{abs}} \tau}{\hbar \omega_p} \right) \frac{2 \sigma L_c}{\pi w^2(z_c)} \int_d^{d+L_g} G_{res}(z'; N) H(z') \, \mathrm{d}z' \tag{10}$$

where σ is the stimulated emission cross section, P_{abs} is the absorbed pump power, $\hbar \omega_p$ is the pump photon energy, τ is the spontaneous emission lifetime, $G_{res}(z'; N)$ is the residual gain distribution of the Nth longitudinal lasing mode, and $H(z')$ is the longitudinal distribution of the normalized pump intensity. In terms of $g(N, d, P_{\mathrm{th}})$, the gain-to-loss ratio for the Nth longitudinal mode is given by

$$\frac{g(N, d, P_{\mathrm{abs}})}{\ln(1/R) + \gamma} = \left(\frac{P_{\mathrm{abs}}}{P_{\mathrm{th}}} \right) L_c \int_d^{d+L_g} G_{res}(z'; N) H(z') \, \mathrm{d}z' \tag{11}$$

where R is the reflectivity of the output coupler, γ is the other round-trip loss, and the threshold pump power P_{th} is
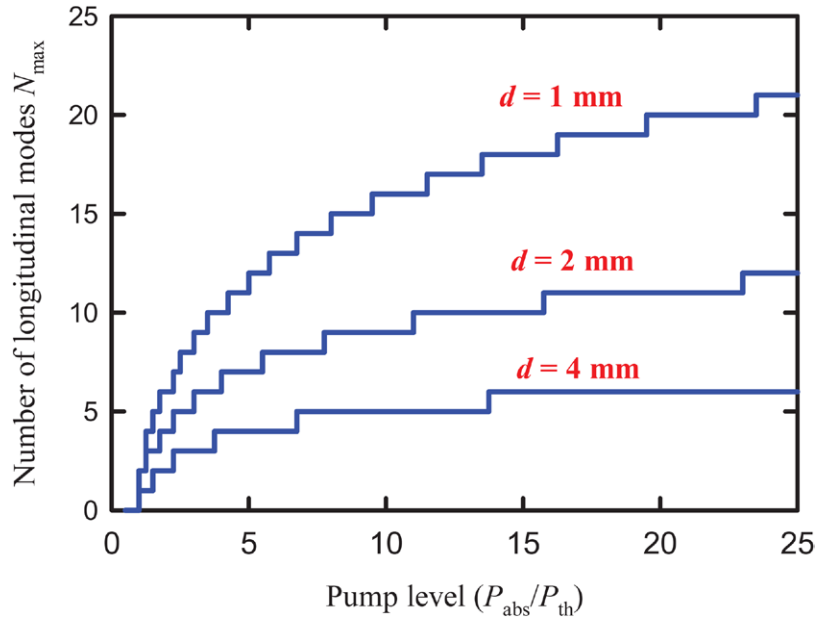
$$P_{\mathrm{th}} = \frac{\pi w^2(z_c)}{2} \cdot \frac{\hbar \omega_p}{\sigma \tau} \left[\ln\left(\frac{1}{R} \right) + \gamma \right]. \tag{12}$$

For a gain medium near the input mirror, the residual gain distribution $G_{res}(z'; N)$ can be approximated as [50]

$$G_{res}(z'; N) = \frac{2}{L_c} \mathrm{e}^{-[N\pi z'/2L_c]^2} \cos^2(k z'). \tag{13}$$

Using the Beer–Lambert law, the normalized pump intensity $H(z')$ is given by

$$H(z') = \frac{\alpha \, \mathrm{e}^{-\alpha(z'-d)}}{1 - \mathrm{e}^{-L_g \alpha}} \tag{14}$$

Figure 2. Calculated results for the dependence of N_{max} on the pump level P_{abs}/P_{th} and the mirror/crystal separation d for a typical case of a diode-pumped Nd:YVO$_4$ laser with $\alpha = 0.5$ mm^{-1}, $L_g = 6$ mm, and $L_c = 30$ mm.

where α is the absorption coefficient at the pump wavelength. Substituting equations (13) and (14) into equation (11) and using $\lambda << L_g$, the gain-to-loss ratio for the Nth longitudinal mode can be approximately derived as an analytical form:

$$\frac{g(N,d,P_{abs})}{\ln(1/R)+\gamma} = \left(\frac{P_{abs}}{P_{th}}\right)\left(\frac{L_c\alpha}{1-e^{-L_g\alpha}}\right)\exp\left[\left(\frac{\alpha L_c}{N\pi}\right)^2 + \alpha d\right]$$

$$\times \frac{1}{N\sqrt{\pi}}\left\{\text{erf}\left[\frac{N\pi(d+L_g)}{2L_c}+\frac{\alpha L_c}{N\pi}\right] - \text{erf}\left[\frac{N\pi d}{2L_c}+\frac{\alpha L_c}{N\pi}\right]\right\}. \tag{15}$$

The maximum number of longitudinal lasing modes N_{max} can then be determined by the condition that the maximum value of N can lead to $g(N,d,P_{abs}) \geqslant \ln(1/R)+\gamma$. Namely,

$$N_{max}(d,P_{abs}/P_{th}) = \left.\frac{g(N,d,P_{abs})}{\ln(1/R)+\gamma}\right|_{N=N_{max}} \geqslant 1. \tag{16}$$

From equations (15) and (16), it can be found that N_{max} is a function of the pump level P_{abs}/P_{th} and the crystal/mirror separation d for a given absorption coefficient α, crystal length L_g, and cavity length L_c.

To reveal the dependence of N_{max} on P_{abs}/P_{th} and d, we performed a numerical calculation for a typical case of a diode-pumped Nd:YVO$_4$ laser in which $\alpha = 0.5$ mm^{-1}, $L_g = 6$ mm, and $L_c = 30$ mm. Calculated results are shown figure 2. The dependence of the maximum longitudinal mode number N_{max} on the pump level P_{abs}/P_{th} can be obviously seen to display a staircase form. Furthermore, it is clear that a smaller the crystal/mirror separation d can lead to more longitudinal modes to get lasing.

III. Representation of wave packet states

To obtain an analytical wave representation for manifesting the wave packet dynamics, the relative amplitude for the

coefficient c_ℓ is modeled as the binomial distribution. Using a new index $j = \ell - \ell_o$ for concise expression, the amplitude coefficient c_j is given by

$$c_j = \frac{1}{2^{N-1}}\frac{(N-1)!}{j!(N-1-j)!} \tag{17}$$

where the factor $1/2^{N-1}$ is included for normalizing the wave function. Substituting equations (9) and (17) into equation (6) and using the property of the Schrödinger coherent state, the wave functions $\Psi^{(\pm)}(x,y,z,t)$ can be deduced as

$$\Psi^{(\pm)}(x,y,z,t) = \sqrt{\frac{2}{\pi w^2(z)}} \exp(-i\,\Theta^{(\pm)}(\tilde{x},\tilde{y},\tilde{z},t))$$

$$\times [\cos(\theta_L^{(\pm)}(\tilde{z},t)/2)]^{N-1}$$

$$\times \exp\left\{-\frac{1}{2}\left(\tilde{x}-\sqrt{2}\sqrt{n_o}\cos[\theta_T^{(\pm)}(\tilde{z},t)\mp\theta_G(z)]\right)^2\right\}$$

$$\times \exp\left\{-\frac{1}{2}\left(\tilde{y}-\sqrt{2}\sqrt{m_o}\cos[\theta_T^{(\pm)}(\tilde{z},t)\mp\theta_G(z)]\right)^2\right\} \tag{18}$$

where the phase factor $\Theta^{(\pm)}(\tilde{x},\tilde{y},\tilde{z},t)$ is given by

$$\Theta^{(\pm)}(\tilde{x},\tilde{y},\tilde{z},t)$$
$$= [\ell_o - 1 + N/2]\,\theta_L^{(\pm)}(\tilde{z},t) + \theta_T^{(\pm)}(\tilde{z},t) \mp (\pi/2) \mp \theta_G(z)$$
$$\quad + \tilde{x}\sqrt{2}\sqrt{n_o}\sin[\theta_T^{(\pm)}(\tilde{z},t)\mp\theta_G(z)]$$
$$\quad - \left(\frac{n_o}{2}\right)\sin\{2[\theta_T^{(\pm)}(\tilde{z},t)\mp\theta_G(z)]\}$$
$$\quad + \tilde{y}\sqrt{2}\sqrt{m_o}\sin[\theta_T^{(\pm)}(\tilde{z},t)\mp\theta_G(z)]$$
$$\quad - \left(\frac{m_o}{2}\right)\sin\{2[\theta_T^{(\pm)}(\tilde{z},t)\mp\theta_G(z)]\}. \tag{19}$$

Even though the phase factor $\Theta^{(\pm)}(\tilde{x},\tilde{y},\tilde{z},t)$ in equation (19) is somewhat complicated, the genuine behavior of the
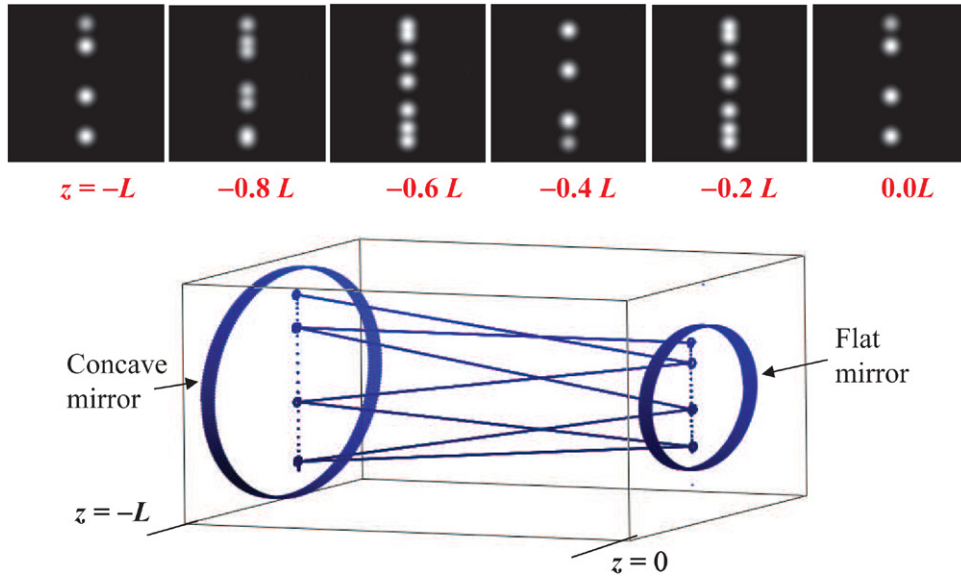
Figure 3. Upper row: numerical transverse patterns for the spatial distribution $I_c(x,y,z)$ at six different longitudinal positions inside the concave-flat resonator with $(P,Q) = (2,7)$, $n_o = 0$, $m_o = 50$, and $R = 30$ mm. Lower row: periodic ray orbit in geometric optics.

wave-packet intensity $|\Psi(x,y,z,t)|^2$ is nearly independent of this factor.

Since the interference between backward $\Psi^{(+)}$ and forward $\Psi^{(-)}$ components only occurs near the reflection mirrors of the cavity, the intensity of the wave-packet state $I = |\Psi(x,y,z,t)|^2$ can be approximately expressed as $I = [I^{(+)} + I^{(-)}]/2$, where

$$I^{(\pm)}(x,y,z,t) = \frac{2}{\pi\, w^2(z)} \left[\cos(\theta_L^{(\pm)}(\tilde{z},t)/2)\right]^{2(N-1)}$$
$$\times \exp\left\{-\left[\tilde{x} - \sqrt{2}\,\sqrt{n_o}\,\cos(\theta_T^{(\pm)}(\tilde{z},t) \mp \theta_G(z))\right]^2\right\}$$
$$\times \exp\left\{-\left[\tilde{y} - \sqrt{2}\,\sqrt{m_o}\,\cos(\theta_T^{(\pm)}(\tilde{z},t) \mp \theta_G(z))\right]^2\right\}.$$
(20)

The analytical form in equation (20) can straightforwardly be exploited to establish the connection between the wave-packet state and the periodic ray orbit. First of all, when the total number of longitudinal modes is fairly greater than one, i.e. $N \gg 1$, the term $\left[\cos(\theta_L^{(\pm)}(\tilde{z},t)/2)\right]^{2(N-1)}$ in equation (20) leads the intensity of the wave packet to exhibit the maxima at $\theta_L^{(\pm)}(\tilde{z},t) = 2\pi s$ for any integers s. Substituting $\theta_L^{(\pm)}(\tilde{z},t) = 2\pi s$ into equation (4) yields $t = s\,t_r \mp (\tilde{z}/c)$. This result indicates that the center of the wave packet $\Psi^{(\pm)}(x,y,z,t)$ in space time $(\tilde{z},t)$ inside the cavity periodically returns to the same position $\tilde{z}$ with a time period of t_r. When the ratio Ω_T/Ω_L is a simple fraction P/Q with P and Q to be co-prime integers, the ray tracing can be used to show that a ray returns exactly to its original position and direction after Q round trips in the cavity and can retrace the same ray pattern to form a closed ray path. Substituting $\theta_L^{(\pm)}(\tilde{z},t) = 2\pi s$ into equation (5) for the cavity with $\Omega_T/\Omega_L = P/Q$, the time-averaged intensity of the wave-packet state $I = |\Psi(x,y,z,t)|^2$ in equation (20)

can be deduced to be localized on the spatial distribution $I_c = [I_c^{(+)} + I_c^{(-)}]/2$ with

$$I_c^{(\pm)}(x,y,z) = \sum_{s=0}^{Q-1} \frac{2}{\pi\, w^2(z)}$$
$$\times \exp\left\{-\left[\tilde{x} - \sqrt{2}\,\sqrt{n_o}\,\cos\left(\frac{P}{Q}2\pi\, s \mp \theta_G(z)\right)\right]^2\right\}$$
$$\times \exp\left\{-\left[\tilde{y} - \sqrt{2}\,\sqrt{m_o}\,\cos\left(\frac{P}{Q}2\pi\, s \mp \theta_G(z)\right)\right]^2\right\}.$$
(21)

Equation (21) reveals that the spatial distribution $I_c(x,y,z)$ of the wave-packet state can be divided into Q parts of backward and forward Gaussian beams. Figure 3 shows the calculated results for the case of the concave-flat resonator with $(P,Q) = (2,7)$, $n_o = 0$, $m_o = 50$, and $R = 30$ mm. Note that the cavity length and the Rayleigh range can be determined by substituting the values of (P,Q) and R into the equations of $L = R\sin^2(P\pi/Q) + [n_r - (1/n_r)]L_g$ and $z_R = L/\tan(P\pi/Q)$, respectively. The upper row in figure 3 depicts the transverse patterns for the spatial distribution $I_c(x,y,z)$ at different six longitudinal positions inside the cavity. It can be seen that the variation of the transverse patterns on the longitudinal positions agrees very well with the periodic ray orbit shown in the lower row in figure 3.

The correspondence between the periodic ray orbit and the spatial distribution $I_c(x,y,z)$ of the wave-packet state can be more explicitly developed by substituting $\tilde{x} = \sqrt{2}\,x/w(z)$ and $\tilde{y} = \sqrt{2}\,y/w(z)$ into equation (21). As a consequence, the mathematical parametric form for the central maxima of backward and forward Gaussian beams in equation (21) can be expressed as
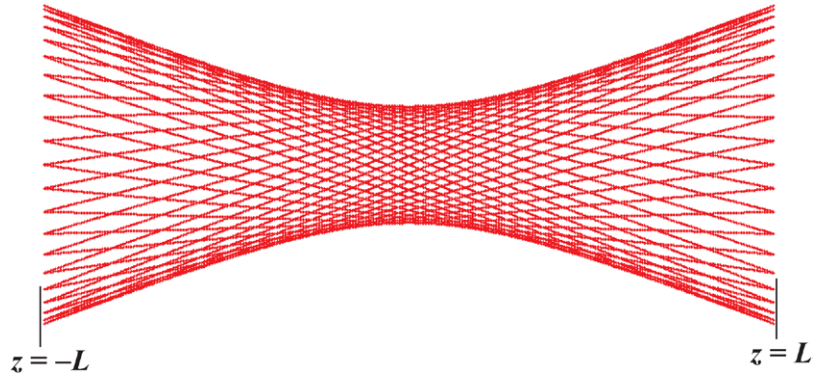
Figure 4. A periodic orbit in the *yz* plane for the cavity with $(P, Q) = (8, 21)$, $n_o = 0$, and $m_o = 50$.
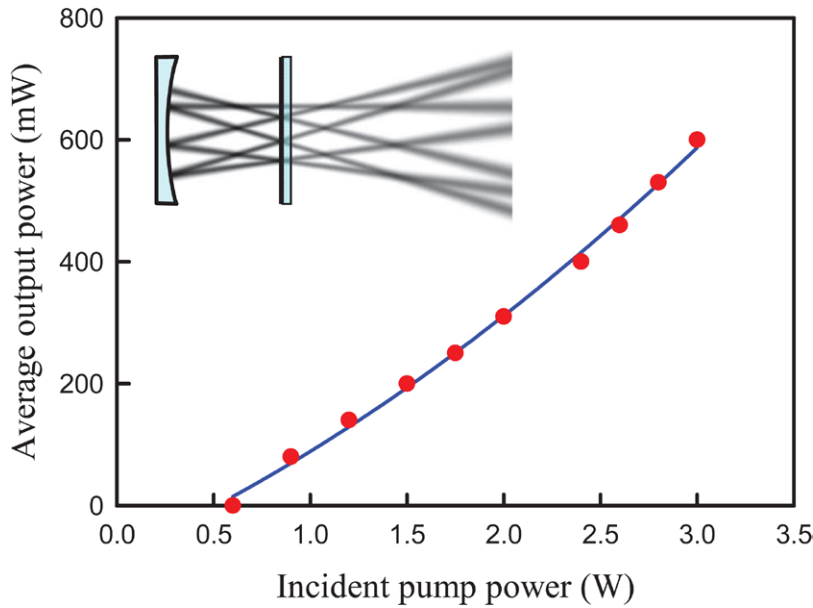
Figure 5. Experimental data for the average output power versus the incident pump power, the inset: the numerical calculation for the intensity of the lasing mode inside the cavity and the propagation of emission.

$$
\begin{cases}
x(z; s) = \sqrt{n_o}\, w(z) \cos\left[\left(\dfrac{P}{Q}\right)(2\pi s) \mp \theta_G(z)\right] \\
y(z; s) = \sqrt{m_o}\, w(z) \cos\left[\left(\dfrac{P}{Q}\right)(2\pi s) \mp \theta_G(z)\right]
\end{cases}
\tag{22}
$$

with $s = 0, 1, \ldots, Q - 1$. Even though the transverse beam width in equation (22) is proportional to $w(z) = w_0\sqrt{1 + (z/z_R)^2}$, the Q-piece trajectories of the periodic ray orbit can be verified to be the straight lines by substituting the Gouy phase $\theta_G(z) = \tan^{-1}(z/z_R)$ into equation (22). With some algebra, the parametric form for the ray trajectories in equation (22) can be rewritten as

$$
\begin{cases}
x(z; s) = \sqrt{n_o}\, w_o \left\{\cos\left[\left(\dfrac{P}{Q}\right)(2\pi s)\right] \pm \left(\dfrac{z}{z_R}\right)\sin\left[\left(\dfrac{P}{Q}\right)(2\pi s)\right]\right\} \\
y(z; s) = \sqrt{m_o}\, w_o \left\{\cos\left[\left(\dfrac{P}{Q}\right)(2\pi s)\right] \pm \left(\dfrac{z}{z_R}\right)\sin\left[\left(\dfrac{P}{Q}\right)(2\pi s)\right]\right\}.
\end{cases}
\tag{23}
$$

Equation (23) clearly reveals that the periodic ray orbit comprises Q-pieces straight lines. Figure 4 depicts a case of the

periodic orbit in the cavity with $(P, Q) = (8, 21)$, $n_o = 0$, and $m_o = 50$ to manifest the subtle connection between hyperbolic caustics and linear trajectories. It is worthwhile to mention that equations (22) and (23) clearly display the role of the Gouy phase in the ray-wave correspondence for the time-dependent wave-packet state in the spherical cavity.

The forward component $I^{(-)}(x, y, z, t)$ in equation (21) can be used to represent the spatio-temporal dynamics of the wave-packet lasing mode emitted from the output coupler. In spatial domain, the output emission with $\Omega_T/\Omega_L = P/Q$ displays a feature of Q multiple Gaussian beams. The temporal dynamics for each far-field Gaussian beam with the index $s = 0, 1, \ldots, Q - 1$ can be derived by substituting the central maxima of equation (22) into equation (20) to yield

$$
\begin{aligned}
I_{out}(z, t; s) = {} & \frac{2}{\pi\, w^2(z)} \left[\cos(\theta_L^{(-)}(z, t)/2)\right]^{2(N-1)} \\
& \times \exp\left\{-2n_o\left[\cos\left(\frac{P}{Q}2\pi s - \theta_G(z)\right) - \cos\left(\frac{P}{Q}\theta_L^{(-)}(z, t) - \theta_G(z)\right)\right]^2\right\} \\
& \times \exp\left\{-2m_o\left[\cos\left(\frac{P}{Q}2\pi s - \theta_G(z)\right) - \cos\left(\frac{P}{Q}\theta_L^{(-)}(z, t) - \theta_G(z)\right)\right]^2\right\}.
\end{aligned}
\tag{24}
$$
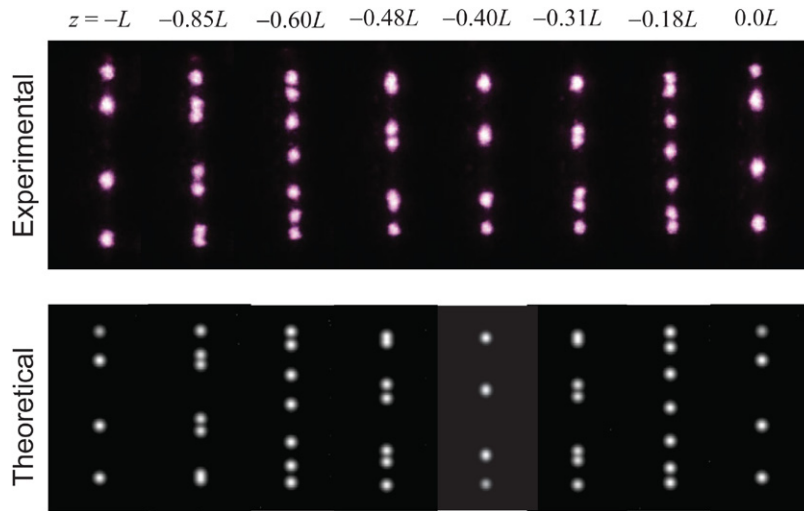
Figure 6. Upper: experimental transverse patterns measured at the different longitudinal positions of the cavity. Lower: theoretical transverse patterns calculated with equation (21) and the parameters $(P, Q) = (2, 7)$, $n_o = 0$, $m_o = 300$, and $R = 30$ mm.
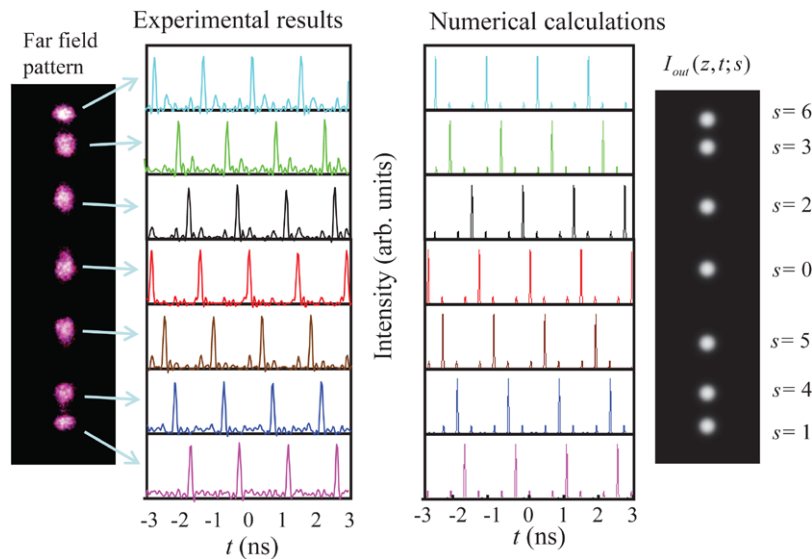
Figure 7. Experimental results for the pulse trains of seven Gaussian spots in the far-field pattern. Theoretical analysis obtained with equation (24) and the parameters are the same as used in figure 6.

In the following, the present theoretical formula is exploited to analyze the experimental results of the total mode-locked states.

IV. Experimental results and numerical analysis

The experimental setup for the total mode-locked operation is a concave-flat cavity with the off-axis pumping scheme, as shown in figure 1. The gain medium is *a*-cut 0.2 at.% Nd:YVO$_4$ crystal with a length of 8 mm. The choice of Nd:YVO$_4$ as medium for laser emission experiments is based on the fact that the YVO$_4$ crystal has a large third-order nonlinearity for an efficiently self-mode-locked operation [36, 38]. The Nd:YVO$_4$ crystal was coated on both end surfaces to be antireflective at 1064 nm ($R < 0.2\%$). Besides, both ends of the laser crystal were wedged 2° to suppress the Fabry–Perot etalon effect. The laser crystal was wrapped with indium foil and mounted in a water-cooled

copper holder to ensure stable laser output. The front mirror was a 30 mm radius-of-curvature concave mirror with antireflection coating at 808 nm on the entrance face and with high-reflectance coating at 1064 nm (>99.8%) and high transmittance coating ($T > 95\%$) at 808 nm on the second surface. The distance between the laser crystal and the front mirror was approximately 2–3 mm. The output coupler was a wedged flat mirror with a reflectivity of 95% at 1064 nm. The pump source was a 3.0 W 808 nm fiber-coupled laser diode with a core diameter of 100 μm and a numerical aperture of 0.16. A lens with a 25 mm focal length was used to focus the pump beam into the laser crystal. The average pump size was approximately 70 μm.

When the optical cavity length L was adjusted to be approximately 32.1 mm, experimental results revealed that a 2D mode-locked state with $(P, Q) = (2, 7)$ could be obtained by using an off-axis displacement 0.4 mm along the *y* direction. Figure 5 depicts experimental data for the average output

power versus the incident pump power. The inset of figure 5 shows the numerical calculation for the intensity of the lasing mode inside the cavity and the propagation of emission. At an incident pump power of 3.0 W, the average output power was measured to be approximately 600 mW. Figure 6 shows experimental transverse patterns measured at the different longitudinal positions of the cavity. Theoretical z-dependent transverse patterns calculated with equation (21) and the parameters $(P, Q) = (2, 7)$, $n_o = 0$, $m_o = 300$, and $R = 30$ mm are also shown in figure 6. It is clear that numerical results agree very well with experimental data.

The far-field pattern of the simultaneously longitudinal and transverse mode-locked laser displays a characteristic of multiple Gaussian spots. We used two high-speed InGaAs photodetectors (Electro-optics Technology Inc. ET-3500 with rise time 35 ps) to identify the time sequence of the mode-locked pulse train via the relative measurement. The first photodetector was employed to measure the temporal behavior in one fixed spot of the far-field pattern for reference. The second photodetector was used to measure the temporal signals in different spots of the far-field pattern for comparison. The output signals of the photodetectors were connected to a digital oscilloscope (Agilent DSO 80000) with 10 GHz electrical bandwidth and a sampling interval of 25 ps. Figure 7 shows the experimental results for the pulse trains of seven Gaussian spots in the far-field pattern. It can be seen that the relative shifts of the time sequences between different spots are wholly consistent with the dynamics of the wave packet traveling along the geometric trajectories inside the cavity. There are some tiny satellite pulses that might come from the presence of the side modes. For comparison, equation (24) is used to calculate the temporal dynamics of the far-field Gaussian beams, where the parameters are the same values adopted in figure 6, the number of longitudinal modes is set to be $N = 8$ from the information of the lasing spectrum, and the distance for the measurement is $z = 28L$. Once again, numerical results agree very well with experimental data. The good agreement between experimental results and theoretical patterns confirms the physical analysis for the total mode-locked state.

V. Conclusions

In summary, the formation of optical wave packet states in the laser resonator has been fully explored by considering the selective pumping and the SHB effect to manifest the time-dependent ray-wave duality. It is theoretically verified that the selective off-axis pumping can excite the transverse modes to be similar to the coherent states of quantum harmonic oscillators. Furthermore, a theoretical formula associated with the SHB effect is derived to analyze the number of the longitudinal lasing modes. By using the determined longitudinal and transverse eigenmodes, the wave function for the total mode-locked state can be analytically derived. The analytical wave function is further used to extract the parametric formula for the periodic trajectories that reveal the subtle relationship between the hyperbolic caustics and linear rays. The

parametric formula and the derived wave function are combined to obtain the temporal dynamics for the output emission of the total mode-locked state. Moreover, a diode-pumped solid-state laser is employed to generate the total mode-locked state. Experimental results are generally found to be in good agreement with numerical analysis based on the derived wave function.

References

[1] Staliunas K and Sanchez-Morcillo V J 2003 *Transverse Patterns in Nonlinear Optical Resonators* (*Spinger Tracts in Modern Physics* vol 183) (Spinger-Verlag)
[2] Okulov A Y 2008 *J. Mod. Opt.* **55** 241–59
[3] Lin Y C, Huang K F and Chen Y F 2013 *Laser Phys.* **23** 115405
[4] Louvergneaux E, Hennequin D, Dangoisse D and Glorieux P 1996 *Phys. Rev.* A **53** 4435
[5] Lin Y C, Lu T H, Huang K F and Chen Y F 2011 *Opt. Express* **19** 10293
[6] Taranenko V B, Staliunas K and Weiss C O 1998 *Phys. Rev. Lett.* **81** 2236
[7] Yu H, Zhang H, Wang Y, Wang Z and Wang J and Petrov V 2013 *Sci. Rep.* **3** 1085
[8] Lee A J, Zhang C, Omatsu T and Pask H M 2014 *Opt. Express* **22** 5400
[9] Dragoman D and Dragoman M 2004 *Quantum-Classical Analogies* (Berlin: Springer)
[10] Huang K F, Chen Y F, Lai H C and Lan Y P 2002 *Phys. Rev. Lett.* **89** 224102
[11] Gensty T, Becker K, Fischer I, Elsäßer W, Degen C, Debernardi P and Bava G P 2005 *Phys. Rev. Lett.* **94** 233901
[12] Chen Y F, Su K W, Lu T H and Huang K F 2006 *Phys. Rev. Lett.* **96** 033905
[13] Galvez E J, Crawford P R, Sztul H I, Pysher M J, Haglin P J and Williams R E 2003 *Phys. Rev. Lett.* **90** 203901
[14] Vorobeichik I, Narevicius E, Rosenblum G, Orenstein M and Moiseyev N 2003 *Phys. Rev. Lett.* **90** 176808
[15] Brand T, Ozygus B and Weber H 1998 *Laser Phys.* **8** 1
[16] Erhard J, Laabs H, Ozygus B and Weber H 1999 Diode-pumped multipath laser oscillators *Proc. SPIE* **3611** 2
[17] Zhang Q, Ozygus B and Weber H 1999 *Eur. Phys. J. Appl. Phys.* **6** 293
[18] Malyutin A A 2007 *Quantum Electron.* **37** 299–306
[19] Chen Y F, Jiang C H, Lan Y P and Huang K F 2004 *Phys. Rev.* A **69** 053807
[20] Schrödinger E 1926 *Naturwissenschaften* **14** 664
[21] Zhang W M, Feng D H and Gillmore R 1990 *Rev. Mod. Phys.* **62** 867
[22] Zurek W H, Habib S and Paz J P 1993 *Phys. Rev. Lett.* **70** 1187
[23] Yeazell J A, Mallalieu M, Parker J and Stroud C R 1989 *Phys. Rev.* A **40** 5040
[24] Lena C, Delande D and Gay J C 1991 *Europhys. Lett.* **15** 697–702
[25] Makowski A J and Górska K J 2007 *J. Phys.* A **40** 11373
[26] Kumar M S and Dutta-Roy B 2008 *J. Phys.* A **41** 075306
[27] Longhi S 2009 *Laser Photon. Rev.* **3** 243
[28] Ramsay I A and Degnan J J 1970 *Appl. Opt.* **9** 385
[29] Auston D H 1968 *IEEE J. Quantum Electron.* **4** 420

[30] Smith P W 1970 *Proc. IEEE* **58** 1342
[31] Krausz F, Brabec T and Spielmann C H 1991 *Opt. Lett.* **16** 235
[32] Liu H, Nees J and Mourou G 2001 *Opt. Lett.* **26** 1723–5
[33] Lagatsky A A *et al* 2005 *Opt. Lett.* **30** 3234–6
[34] Xie G Q, Tang D Y, Zhao L M, Qian L J and Ueda K 2007 *Opt. Lett.* **32** 2741–3
[35] Uemura S and Torizuka K 2008 *Appl. Phys. Express* **1** 012007
[36] Liang H C, Chen R C C, Huang Y J, Su K W and Chen Y F 2008 *Opt. Express* **16** 21149–54
[37] Chen Y F, Liang H C, Tung J C, Su K W, Zhang Y Y, Zhang H J, Yu H H and Wang J Y 2012 *Opt. Lett.* **37** 461–3
[38] Liang H C, Huang Y J, Huang W C, Su K W and Chen Y F 2010 *Opt. Lett.* **35** 4–6
[39] Chen Y F, Lee Y C, Liang H C, Lin K Y, Su K W and Huang K F 2011 *Opt. Lett.* **36** 4581–3
[40] Liang H C, Wu T W, Tung J C, Tsou C H, Huang K F and Chen Y F 2013 *Laser Phys. Lett.* **10** 105804

[41] Haus H A 1984 *Waves and Fields in Optoelectronics* (Englewood Cliffs, NJ: Prentice-Hall) chapter 5
[42] Chen Y F, Tung J C, Chiang P Y, Liang H C and Huang K F 2013 *Phys. Rev.* A **88** 013827
[43] Chen Y F 2011 *Phys. Rev.* A **83** 032124
[44] Fu H and Haken H 1991 *Phys. Rev.* A **43** 2446
[45] Flood C J, Walker D R and van Driel H M 1995 *Opt. Lett.* **20** 58
[46] Kim H S, Kim S K and Kim B Y 1996 *Opt. Lett.* **21** 1144
[47] Jiang L and Asryan L V 2008 *IEEE Photon. Technol. Lett.* **20** 1661
[48] Kintz G J and Baer T 1990 *IEEE J. Quantum Electron.* **26** 1457
[49] Zayhowski J J 1990 *Opt. Lett.* **15** 431
[50] Chen Y F, Huang Y J, Chiang P Y, Lin Y. C and Liang H C 2011 *Appl. Phys.* B **103** 841